

Evaluation of RWM Feedback Connections Based MHD Eigenfunctions

F. Perkins, M. Okabayashi, M. Chance,
M. Chiu, R. Nazikian, A. Turnbull

November 2004

MOTIVATION

- Generalize success of $n=0$ plasma control to feedback of $n=1,2,3$ modes
- Increased fusion performance by operation with $\beta > \beta_{\text{no-wall}}$.
- Kink mode (with growth rate determined by wall resistivity) is the principal instability
- For ITER, fusion power increases from nominal 400 MW to $\sim 800 - 1000$ MW

EIGENFUNCTIONS OF UNSTABLE KINK MODES

- Unstable kink $n = 1$ mode bulges outward in equatorial plane at $\phi = 0$ and has radial magnetic field at $\phi = \pi/2$
- Note up-down symmetry (antisymmetry) for $\phi = 0$ (for $\phi = \pi/2$)
- Actuator coils have window-frame connection

MHD EQUILIBRIA

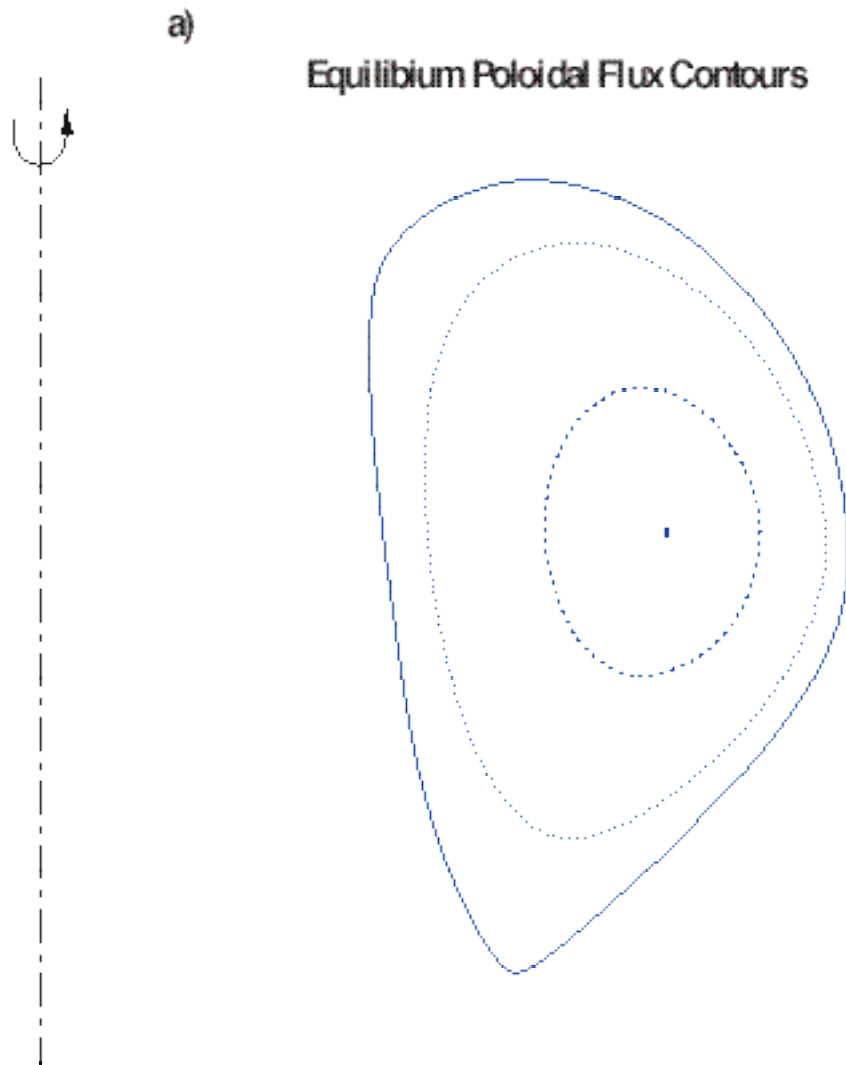


FIG. 2a. Equilibrium flux surfaces for $n=1$ unstable ITER Demonstration Discharge equilibrium with $q_0=1.05$ and $\beta_N = 4.15$. More details concerning this equilibrium and the stability analysis can be found in A. D. Turnbull , et al. Nuclear Fusion **39** 1557 (1999).

EIGEN FUNCTION $\phi=0$

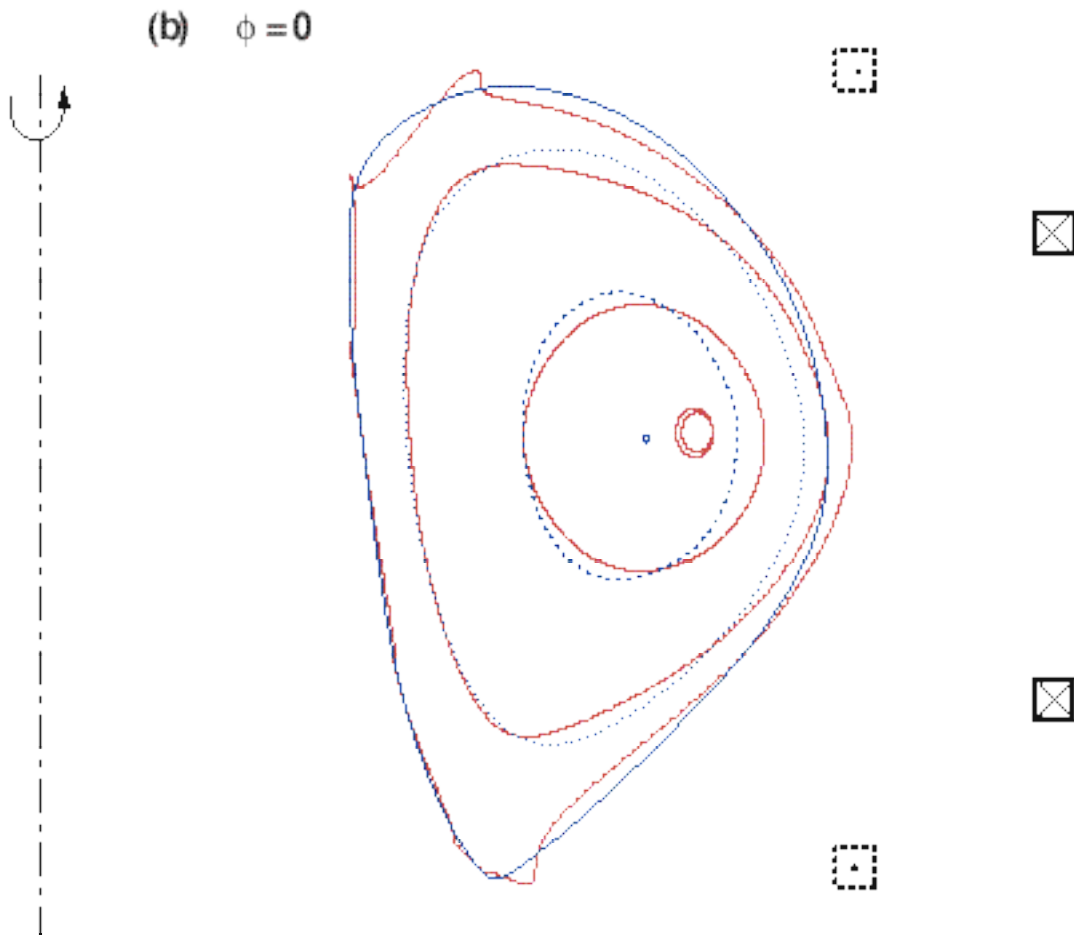


FIG. 2b) Perturbed flux surfaces for $\phi=0$, illustrating outward ballooning in mid-plane. Red surfaces are perturbed; blue is the equilibrium of Fig. 2a). Squares with heavy lines indicate the position of present feedback coils. Dotted squares indicate positions where additional coils would be effective in pushing or pulling the perturbed plasma back toward its equilibrium position. These could be realized by two sets of window frame coils moved off the mid-plane.

EIGEN FUNCTION $\phi=\pi/2$

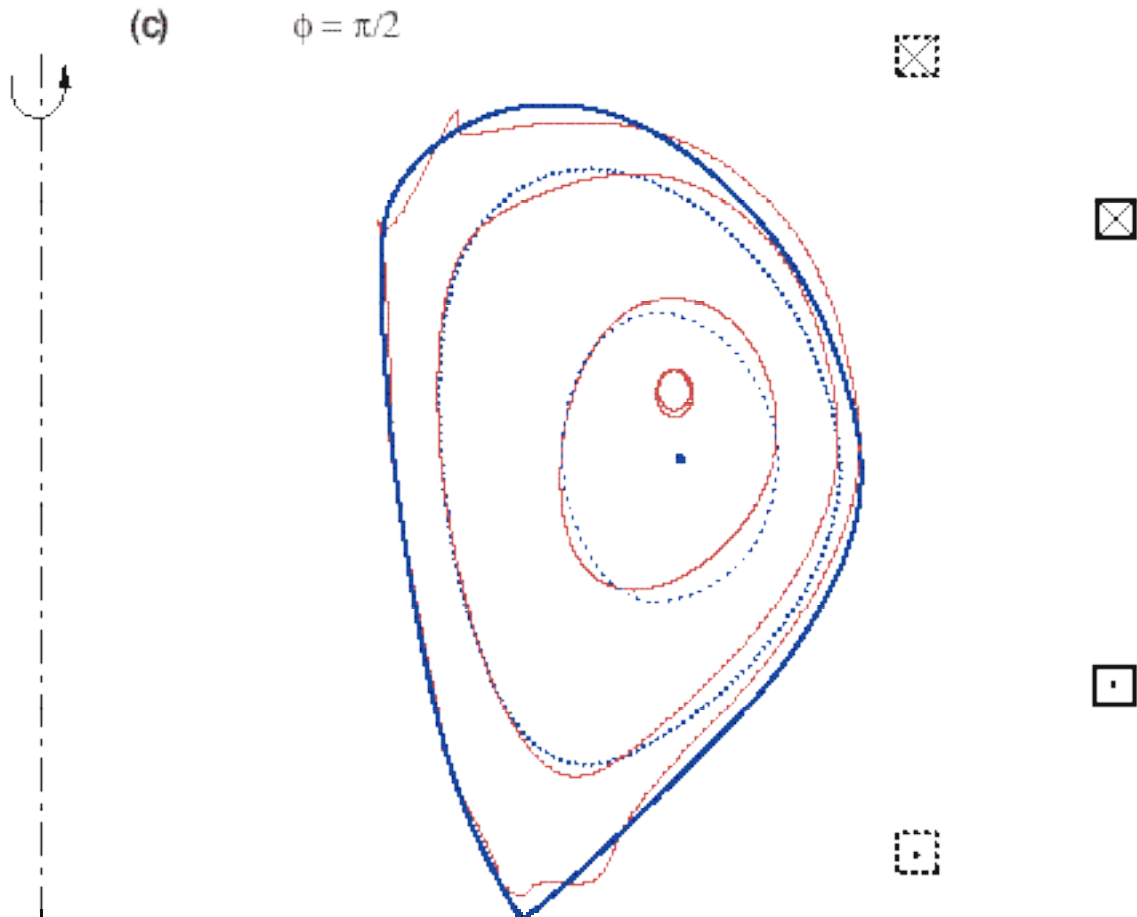
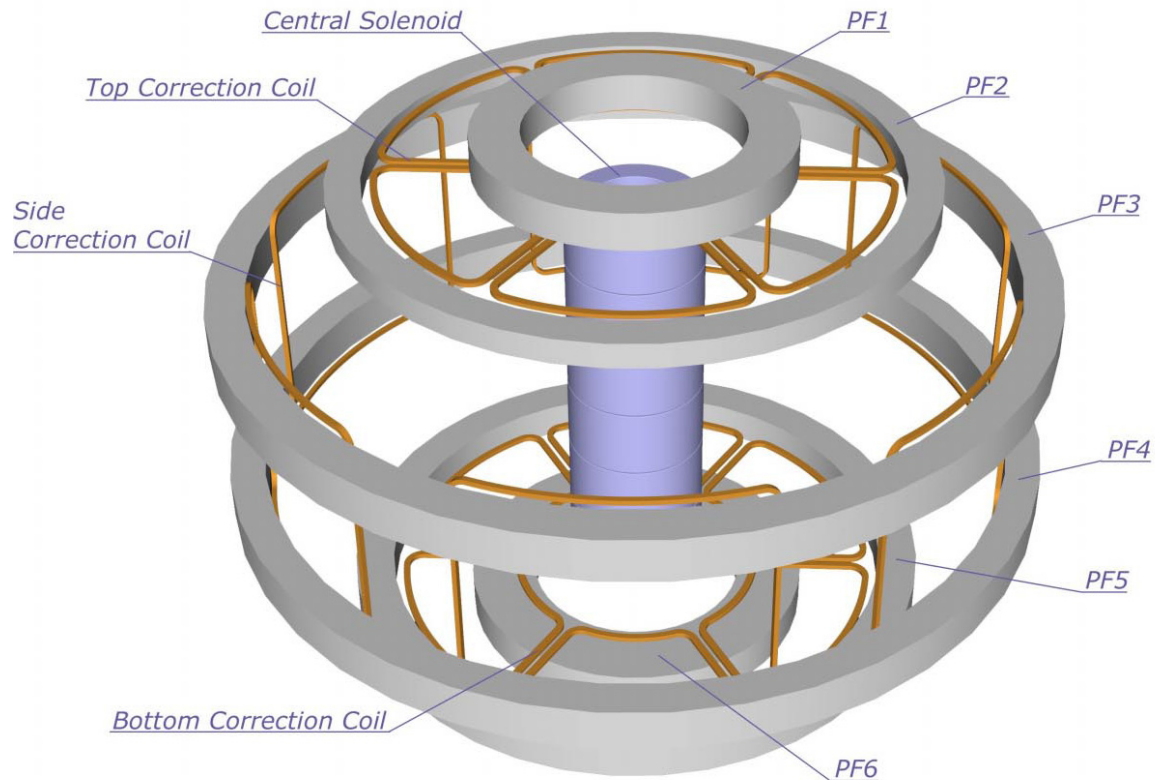


FIG. 2c) Perturbed flux surfaces for $\phi=\pi/2$, illustrating radial field in mid-plane. Red surfaces are perturbed; blue is the equilibrium of Fig. 2a). Squares with heavy lines indicate the position of present feedback coils. Dotted squares indicate positions where additional coils would be effective in pushing or pulling the perturbed plasma back toward its equilibrium position.

ITER SINGLE-BELT COILS

ITER FEAT - PF Coil System



ACTUATOR COILS

- **Window pane connection (up-down antisymmetric)**

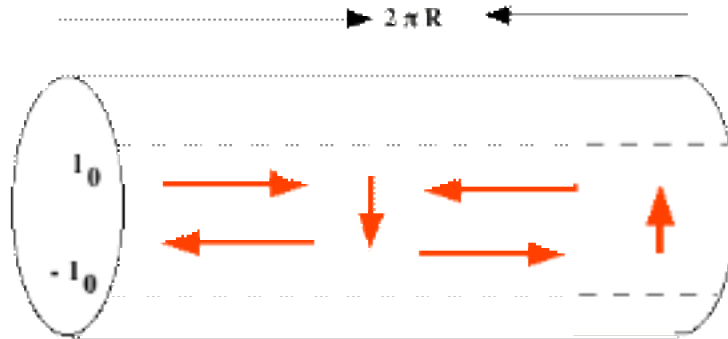


FIG. 4. Sketch of $n=1$ standard window pane current sheet.

- **Alternative Connection (up-down symmetric)**

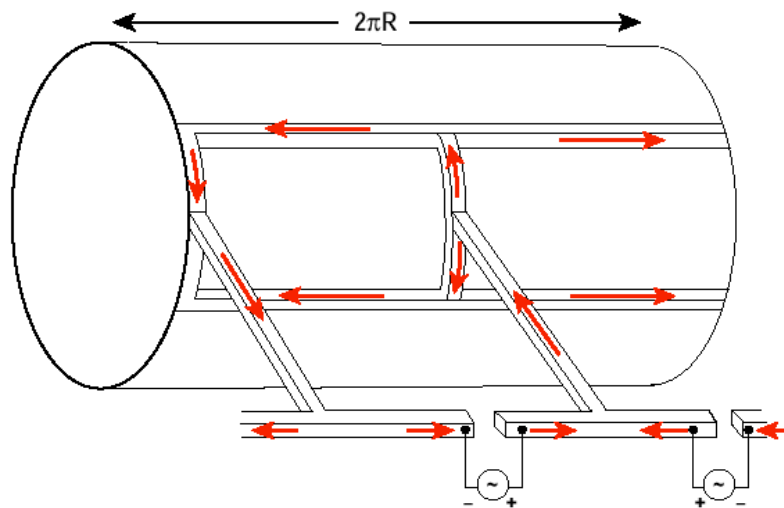
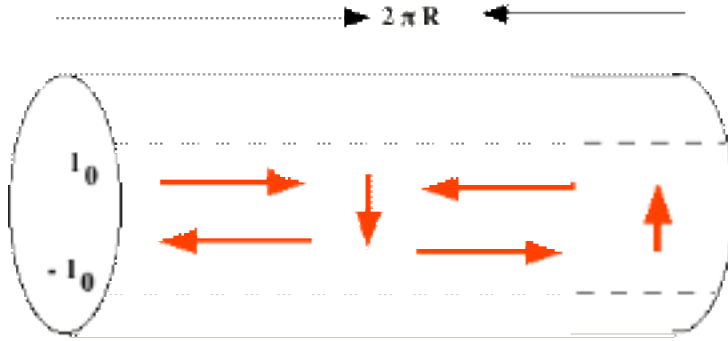


FIG. 1. Alternative Connection Scheme for $n=1$



• **Model for Window PanerConnection.** For DIII-D coils, the current sheet should lie in the magnetic surface labeled by $R=3.0$ m in the midplane and the sheet should extend to 0.7m above (and below) midplane. For the alternative winding case the current in the sheet is not divergence-free and an additional sheet lying in the midplane is required as illustrated in Figure (5).

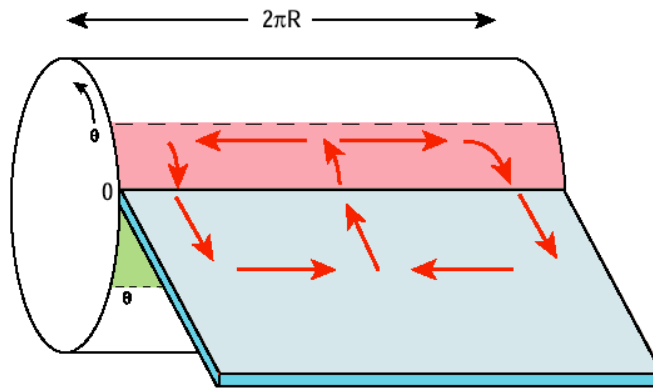


FIG. 5 Sketch of $n=1$ alternative current sheet

• **Model for Alternative Connection.** The current in the sheet is driven to be proportional to the sensor amplitude multiplied by a gain and phase shift as discussed below. Integral or derivative feedback couplings could be considered as well.

Mathematically, the current model for the standard window frame coils is

$$\mathbf{J} = \left(-\frac{\partial I}{\partial \ell} \hat{\phi} + \frac{i n}{R} I \hat{\theta} \right) e^{in(\phi - \phi_0)} \quad -\ell_0 < \ell < \ell_0 \quad (1)$$

where I should be an even function of ℓ and should vanish at $\ell = \pm \ell_0$. An ad-hoc choice for $I(\ell)$ is

$$I = I_0 \left(1 - \frac{z^2}{l_0^2}\right)^{m_1} \quad -l_0 < z < l_0 \quad . \quad (2)$$

$$I = 0 \quad \text{otherwise}$$

Here I_0 parametrizes the total current flowing in the sheet and m_1 governs its spatial distribution. A value $m_1 = 0.25$ is suggested so that most of the toroidal current flows near the the upper and lower boundaries of the current sheet, mimicking the discrete coil conductors.

To model the alternative coils, the sheet current must reverse sign as $\ell = 0$ is crossed. The model is

$$\mathbf{J} = \left(-\frac{\partial I}{\partial \ell} \hat{\phi} + \frac{i n}{R} I \hat{\theta} \right) e^{i n(\phi - \phi_0)} \quad 0 < \ell < \ell_0 \quad (3)$$

$$\mathbf{J} = \left(\frac{\partial I}{\partial \ell} \hat{\phi} - \frac{i n}{R} I \hat{\theta} \right) e^{i n(\phi - \phi_0)} \quad -\ell_0 < \ell < 0 \quad (4)$$

$$\mathbf{J} = 0 \quad \text{Otherwise} \quad (5)$$

The current distribution (3-5) is not divergence-free; currents flow toward $\ell = 0$ in both the upper and lower sheets. Therefore, an additional current sheet lying in the equatorial plane is invoked for $R_0 < R < R_1$. This current sheet has the form

$$\mathbf{J} = 2 \left(-\frac{\partial F}{\partial R} \hat{\phi} + i \frac{n}{R} F \hat{\mathbf{R}} \right) e^{i n(\phi - \phi_0)} \quad R_0 < R < R_1 \quad (6)$$

$$\mathbf{J} = 0 \quad \text{Otherwise}$$

where the function $F(R)$ is

$$F = I_0 \left[1 - \left(\frac{R - R_0}{R_1 - R_0} \right)^2 \right]^{m_2} \quad R_0 < R < R_1 \quad (7)$$

As before, $m_2 = 0.25$ will place the return toroidal current near the outer edge of this current sheet. For initial studies, take $R_1 = 2 R_0$. Taken together, equations (3)-(7) produce a divergence free, $n=1$ sheet current distribution that models the alternative feedback currents.

Actuator Waveforms.

Time waveforms for each of the twelve window pane coils installed on DIII-D follow from the above arguments. The waveforms for current in the m^{th} coil set depend on the toroidal angle $\phi_m = \Omega t - \phi_0 - m\pi/3$ where $m=0, 1, \dots, 5$. Here, Ω denotes the plasma rotation rate

$$\begin{aligned} C1_m &= I\{\cos(\phi_m) + \sin(\phi_m)\} \\ C2_m &= -I\{\cos(\phi_m) + \sin(\phi_m)\} \\ C3_m &= -I\{\cos(\phi_m) - \sin(\phi_m)\} \\ C4_m &= I\{\cos(\phi_m) - \sin(\phi_m)\} \end{aligned} \tag{1}$$

Sensors. The sensor network foreseen is extensive and consists of six modules, one for each coil location. As illustrated in Fig.2, each module in turn has 3 measuring locations — above-, on-, and below- midplane — as well as two polarizations — poloidal and radial. Altogether, there are 36 diagnostics signals for use in determining the actuator currents. Figure 5 summarizes their properties and origin.

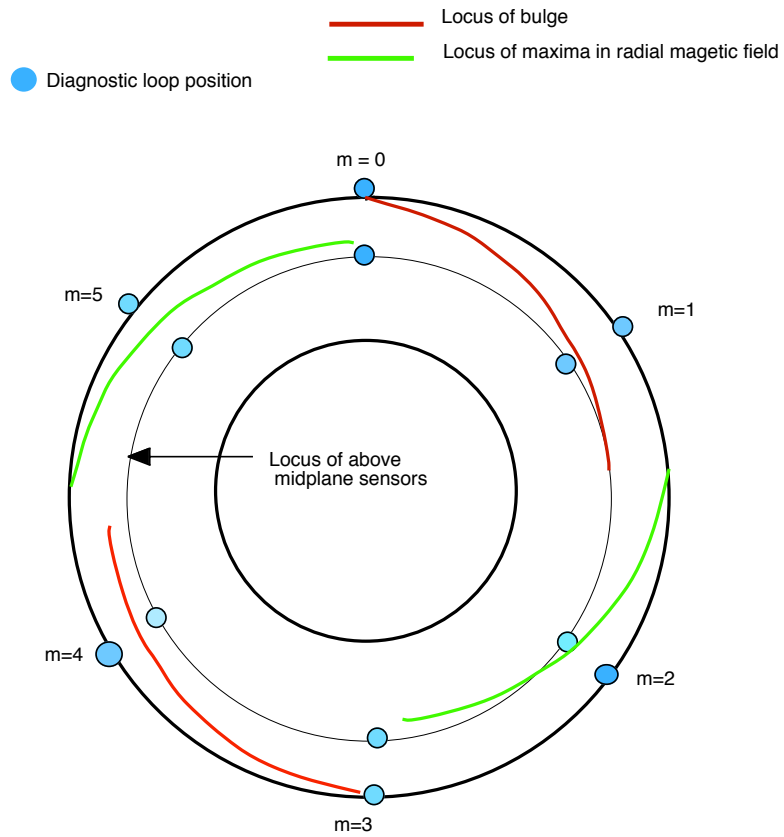


FIG.5. Diagnostic loop positions and $n=1$ wall-stabilized eigenfunctions. Red and green curves correspond to Fig.4.

CONCLUSIONS

- With standard and alternative connections, a one belt set of coils will be as effective as a two belt system with only window-pane connections.
- Sensor systems should exploit polarization and use eigenmode phase relations
- Geometry Similar to ITER Error field Correction Coils